Available online at www.sciencedirect.com
SCIENCE DIRECT®
Journal of Solid State Chemistry 177 (2004) 1575–1584
JOURNAL OF SOLID STATE CHEMISTRY
http://elsevier.com/locate/jssc

Structure and phase transitions in $[(CH_3)_4P]_3[Sb_2Br_9]$ and $[(CH_3)_4P]_3[Bi_2Br_9]$

M. Wojtaś,[a] R. Jakubas,[a,*] Z. Ciunik,[a] and W. Medycki[b]

[a] *Department of Chemistry, University of Wrocław, Joliot-Curie 14, 50-383 Wrocław, Poland*
[b] *Institute of Molecular Physics, Polish Academy of Science, Smoluchowskiego 17, 60-179 Poznań, Poland*

Received 19 August 2003; received in revised form 3 December 2003; accepted 9 December 2003

Abstract

Two new phosphonium bromoantimonate(III) and bromobismuthate(III) $[(CH_3)_4P]_3[Sb_2Br_9]$ (PBA) and $[(CH_3)_4P]_3[Bi_2Br_9]$ (PBB) crystals have been synthesized and their structure determined by single-crystal X-ray diffraction. Both compounds are isomorphous in the room temperature phase and crystallize in the trigonal space group (polar), $P31c$. The structure consists of discrete $[M_2X_9]^{3-}$ anions and $[(CH_3)_4P]^+$ cations. A sequence of structural phase transitions in PBA and PBB is established on the basis of differential scanning calorimetry and dilatometric studies. Two reversible phase transitions are found: (I↔II) at 540/540 K and (II↔III) at 193/195 K for PBA and (I↔II) at 550/550 K and (II↔III) at 205/207.5 K for PBB (on cooling/heating). The pyroelectric measurements of both compounds have confirmed the polar nature of phases (II) and (III). Proton spin–lattice relaxation time of polycrystalline PBA have been studied in temperatures 77–400 K. A dynamic inequivalence of two tetramethylphosphonium cations has been detected. A ferroelastic domain structure was found over the lowest temperature phase (III) of both crystals studied. The possible mechanisms of the phase transitions are discussed on the basis of the presented results.
© 2003 Elsevier Inc. All rights reserved.

Keywords: Halogenobismuthate(III) and halogenoantimonate(III); Structure; Phase transition; Ferroelastic

1. Introduction

The halogenoantimonates(III) and halogenobismuthates(III) of a general formula $R_aM_bX_{(3b+a)}$ (R = alkylammonium cations; M = Sb and Bi; X = Cl, Br, I) are well known for interesting phase transitions, ferroelastic and ferroelectric properties and modulated incommensurate phases [1–6]. From among these salts, which are characterized by various anionic forms, the ones with the $R_3M_2X_9$ and $R_5M_2X_{11}$ compositions deserve special attention because they frequently demonstrate ferroelectric and ferroelastic properties. Their anionic $[M_2X_9]^{3-}$ sublattice is composed of: (i) one-dimensional zigzag chains [7], (ii) two-dimensional layers [8], and (iii) discrete bioctahedral [9]. It has turned out that an appearance of ferroelectricity is limited to salts with small-sized cations like: $[CH_3NH_3]^+$, $[(CH_3)_2NH_2]^+$ and $[(CH_3)_3NH]^+$ embedded in layer anionic structure (type (ii)). In turn, the $R_5M_2X_{11}$-type salts are extremely rare [10]. Up to now only three salts with this composition with methylammonium and pyridinium cations were synthesized and all of them possess ferroelectric properties. Both classes of these crystals are classified as the order–disorder ferroelectrics for which the mechanism of phase transitions is governed by the dynamics of organic cations. Quite recently a novel ferroelectric with RSbCl$_4$ composition, (4-NH_2PyHSbCl$_4$), characterized by one-dimensional anionic form, $(SbCl_4^-)_\infty$ has been discovered [11]. It is a unique structurally incommensurate (IC) ferroelectric crystal with the complex sequence of phase transitions [12].

In the case of salts with $R_3M_2X_9$ composition it was shown that the type of structure adopted by $[M_2X_9]^{3-}$ anions depends on the size of the cations and the possibility of specific interactions with the anion. Large bulky cations like tetramethylammonium inhibit the formation of a polymeric anion (steric effect and extremely weak specific interaction) in the crystal lattice and as a result only the bioctahedral anionic structure is formed. The all halogenoantimonates(III) and halogenobismuthates(III) tetramethylammonium salts studied by us are devoid of ferroelectric properties; however,

*Corresponding author. Fax: +48-71-328-2348.
E-mail address: rj@wchuwr.chem.uni.wroc.pl (R. Jakubas).

0022-4596/$ - see front matter © 2003 Elsevier Inc. All rights reserved.
doi:10.1016/j.jssc.2003.12.011

they undergo low-temperature transitions to the ferroelastic phases and pyroelectric properties are also possible.

It would be interesting to replace the central nitrogen atoms of the cation with higher pnicogens, Pn =P, As and Sb to extend the family of halogenoantimonates(III) and halogenobismuthates(III), $[(CH_3)_4Pn]_a[M_bX_{3b+a}]$. To the best of our knowledge, no phosphonium halogenoantimonates(III) or halogenobismuthates(III) as ionic salts have been reported.

In this paper we report on the structural properties of the two new members of the $R_aM_bX_{(3b+a)}$ family of crystals: $[(CH_3)_4P]_3[Sb_2Br_9]$ and $[(CH_3)_4P]_3[Bi_2Br_9]$. The compounds exhibit phase transitions in the low- and high-temperature region. The phase transition sequence is characterized using differential scanning calorimetry (DSC), dilatometry, dielectric and pyroelectric methods. The molecular motions in the $[(CH_3)_4P]_3[Sb_2Br_9]$ crystal were studied by proton nuclear magnetic resonance (^{1}H NMR).

2. Experimental

Powders of tris(tetramethylphosphonium) nonabromodiantimonate(III), $[(CH_3)_4P]_3[Sb_2Br_9]$ (PBA), and tris(tetramethylphosphonium) nonabromodibismuthate(III) $[(CH_3)_4P]_3[Bi_2Br_9]$ (PBB) were obtained by dissolving a mixture (in molar ratio 1:1) of $[(CH_3)_4P]$Br (Aldrich, 98%) and $SbBr_3$ (PBA—Aldrich 99.99%) or $BiBr_3$ (PBB—Aldrich, 98%) in a concentrated HBr (Aldrich, 48%). The resulting transparent, air-stable and deep yellow polycrystals of PBA and PBB were recrystallized twice from acid solution. The single crystals of PBA or PBB were grown by a slow evaporation of an acid solution (20% HBr) at room temperature. The crystals grow in a pseudo-hexagonal manner and have a well-developed (001) plane.

The amount of tetramethylphosphine in PBA and PBB determined by elemental analysis of the samples agrees well with the proposed formula; found for PBA: C, 11.78%; H, 2.80%; theoretical (PBA): C, 11.65%; H, 2.91%; and found for PBB: C, 10.36%; H, 2.24%; theoretical (PBB): C, 10.21%; H, 2.55%.

Crystal data are given in Table 1, together with refinement details. All measurements of crystals were performed on a Kuma KM4CCD κ-axis diffractometer with graphite-monochromated Mo$K\alpha$ radiation. Crystals were positioned at 65 mm from the KM4CCD camera. Six hundred and twelve frames were measured at 0.75° intervals with a counting time of 20 s. The data were corrected for Lorentz and polarization effects. Analytical absorption corrections, data reduction and analysis were carried out with the Oxford Diffraction (Poland) programs. Structures were solved by the heavy atom method (program SHELXS97 [13]) and refined by the full-matrix least-squares method on all F^2 data using the SHELXL97 [14] programs. Non-hydrogen atoms were refined with anisotropic displacement parameters; hydrogen atoms were included from the geometry of molecules and $\Delta\rho$ maps but were fixed.

The atomic coordinates and equivalent isotropic displacement parameters for $[(CH_3)_4P]_3[Sb_2Br_9]$ and $[(CH_3)_4P]_3[Bi_2Br_9]$ are given in Table 2. Crystallographic

Table 1
Crystal data and structure refinement for $[(CH_3)_4P]_3[Sb_2Br_9]$ and $[(CH_3)_4P]_3[Bi_2Br_9]$

Empirical formula	$[(CH_3)_4P]_3[Sb_2Br_9]$		$[(CH_3)_4P]_3[Bi_2Br_9]$
Formula weight	1236.01		1410.47
Temperature (K)		293(2)	
Wavelength (Å)		0.71073	
Crystal system		Trigonal	
Space group		$P31c$	
Unit-cell dimensions	$a = 9.7931(7)$ Å		$a = 9.7880(12)$ Å
	$c = 22.6974(19)$ Å		$c = 22.840(4)$ Å
Volume [Å^3]	1885.2(2)		1895.0(4)
Z		2	
Calculated density (g cm^{-3})	2.177		2.472
Absorption coefficient (mm^{-1})	11.100		18.890
$F(000)$	1140		1268
Crystal size (mm)	$0.10 \times 0.10 \times 0.10$		$0.31 \times 0.21 \times 0.09$
Theta range for data collection (deg)	3.59–28.41		3.60–28.46
Ranges of h, k, l	$-13 \Rightarrow 12, -12 \Rightarrow 12, -23 \Rightarrow 29$		$-11 \Rightarrow 13, -12 \Rightarrow 11, -30 \Rightarrow 28$
Reflections collected	12372		12467
Independent reflections (R_{int})	2651 (0.1047)		2940 (0.1209)
Absorption correction		Analytical	
Data/parameters	2651/73		2940/72
Goodness-of-fit on F^2	1.091		1.046
Final R_1/wR_2 indices ($I > 2\sigma I$)	0.0683/0.1323		0.0635/0.1089
Largest diff. peak/hole (e Å^{-3})	0.968/ − 0.770		1.040/ − 1.105

Table 2
Atomic coordinates and equivalent isotropic displacement parameters ($Å^2$) for $[(CH_3)_4P]_3[Sb_2Br_9]$ and $[(CH_3)_4P]_3[Bi_2Br_9]$

Atom	x	y	z	U_{eq}
$[(CH_3)_4P]_3[Sb_2Br_9]$				
Sb1	0.3333	0.6667	0.62102(8)	0.0631(5)
Sb2	0.3333	0.6667	0.44775(7)	0.0635(5)
Br3	0.41835(18)	0.48510(17)	0.53419(11)	0.0889(6)
Br4	0.2575(3)	0.8428(3)	0.68574(11)	0.1039(7)
Br5	0.5851(2)	0.7425(3)	0.38290(11)	0.1035(7)
P1	0.6667	0.3333	0.3747(3)	0.0617(19)
P2	0.6667	1.3333	0.6931(3)	0.063(2)
P3	0	0	0.5323(4)	0.0675(14)
C11	0.6667	0.3333	0.4580(14)	0.126(14)
C12	0.813(3)	0.516(2)	0.3473(11)	0.130(8)
C21	0.6667	1.3333	0.6212(15)	0.098(10)
C22	0.690(3)	1.177(3)	0.7195(11)	0.137(10)
C31	−0.044(3)	0.157(3)	0.5609(8)	0.187(12)
C32	0	0	0.4553(4)	0.29(4)
$[(CH_3)_4P]_3[Bi_2Br_9]$				
Bi1	0.3333	0.6667	0.62204(5)	0.0619(4)
Bi2	0.3333	0.6667	0.44646(5)	0.0617(4)
Br3	0.4189(2)	0.48864(18)	0.53400(11)	0.0742(5)
Br4	0.2538(3)	0.8488(3)	0.68668(13)	0.1011(8)
Br5	0.5952(3)	0.7457(3)	0.38171(12)	0.1016(8)
P1	0.6667	0.3333	0.3736(4)	0.055(2)
P2	0.6667	1.3333	0.6954(5)	0.066(3)
P3	0	0	0.5315(5)	0.0647(17)
C11	0.6667	0.3333	0.452(2)	0.106(15)
C12	0.814(3)	0.520(2)	0.3466(13)	0.121(9)
C21	0.6667	1.3333	0.619(2)	0.122(17)
C22	0.690(3)	1.173(3)	0.7189(16)	0.141(11)
C31	−0.045(4)	0.172(5)	0.5552(15)	0.235(18)
C32	0	0	0.4552(5)	0.32(5)

U_{eq} is defined as one-third of the trace of the orthogonalized U_{ij} tensor.

data for the structures reported in this paper (excluding structure factors) have been deposited with the Cambridge Crystallographic Data Centre, CCDC no. 214330 (PBA) and 214331 (PBB). Copies of this information may be obtained free of charge from the Director, CCDC, 12 UNION Road, Cambridge 1EZ UK (fax: +44-1223-336033; e-mail: deposit@ccdc.cam.ac.uk, http://www.ccdc.cam.ac.uk).

The complex electric permittivity, $\varepsilon^* = \varepsilon' - i\varepsilon''$, was measured by an HP 4284 and HP 4285A Precision LCR Meters in the frequency range between 1 kHz and 25 MHz and in the temperature range between 100 and 400 K. The dimensions of the sample were of the order of $2 \times 3 \times 1$ mm^3. The overall error for the real and imaginary parts of the complex electric permittivity was less than 5% and 10%, respectively.

The pyroelectric charge was measured by a KEITHLEY 617 electrometer. Differential scanning calorimetry (DSC) measurements were carried out using a Perkin-Elmer DSC-7 in the temperature range 100–570 K.

Thermogravimetric analyses (TGA) and differential thermal analyses (DTA) were performed on a Setaram SETSYS 16/18 instrument in nitrogen atmosphere, sample mass: 10 mg; heating rate 2 K min^{-1}, in the temperature range 300–750 K.

The dilatometric measurements were performed by a thermomechanical analyzer Perkin-Elmer TMA-7 in the temperature range 100–590 K. The dimensions of the sample were of the order of $2 \times 3 \times 1$ mm^3.

The ferroelastic domain structure of the crystal was studied by means of a OLYMPUS (BX60 SYSTEM) optical polarization microscope. The samples were placed in a LINKAM THM-600 heating–cooling stage where the temperature was stabilized to within 0.01 K.

The measurements of ^{1}H spin–lattice relaxation time (T_1) were made at 90 MHz with a pulsed Bruker SXP 4-100 spectrometer. The relaxation time was determined by applying a conventional π–τ–$\pi/2$ pulse sequence. The crystal was powdered for measurements. The sample temperatures were obtained by employing a nitrogen gas flow system equipped with a Bruker BS 100/700 temperature controller. The temperature of the sample was controlled to an accuracy of 1 K.

3. Results and discussion

3.1. X-ray results

The structure of both title crystals is characterized by moderating state of refinement. It is caused by the disorder forced on the tetramethylphosphonium cations by the trigonal space group symmetry. We should add that the pure refinements have been obtained previously for a similar type of compounds: $[(CH_3)_4N]_3[Sb_2Br_9]$ (the final $R = 0.14$), $[(CH_3)_4N]_3[Sb_2Br_3Cl_6]$ ($R = 0.115$) [15], crystallizing in the hexagonal symmetry.

For the room temperature phase the structure solution of PBA yielded the coordinates of the discrete $[Sb_2Br_9]^{3-}$ anion and the three crystallographically independent tetramethylphosphonium cations (Fig. 1).

No disorder of the cations was resolvable, although the large values obtained for the carbon atom displacement parameters indicate a large amount of thermal motion, especially for the cations type (3). Final atomic coordinates of PBA and PBB are given in Table 2.

Bond lengths of anions and cations are given in Table 3. The geometry of the antimony and bismuth atoms is basically octahedral with no stereochemical position for the lone pair electrons. Because of the high symmetry the anions $[M_2Br_9]^{3-}$ are defined by only two metal–bromine distances associated with the bridging and terminal atoms, respectively. There is no significant deviation in the bond angles and distances of the $[Sb_2Br_9]^{3-}$ and $[Bi_2Br_9]^{3-}$ anions from the values in similar structures reported in the literature [16,17]. The anionic structure along the b-axis as a polyhedral representation is depicted in Fig. 2. Factors influencing

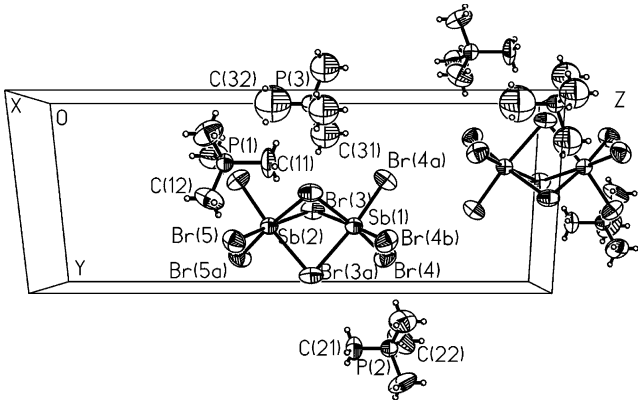

Fig. 1. Perspective view of the crystal structure of PBA along the *a*-axis.

Table 3
Bond lengths (Å) for $[(CH_3)_4P]_3[Sb_2Br_9]$ and $[(CH_3)_4P]_3[Bi_2Br_9]$

$[(CH_3)_4P]_3[Sb_2Br_9]$		$[(CH_3)_4P]_3[Bi_2Br_9]$	
Sb(1)–Br(4)	2.639(2)	Bi(1)–Br(4)	2.711(2)
Sb(1)–Br(3)	3.036(2)	Bi(1)–Br(3)	3.040(2)
Sb(2)–Br(5)	2.639(2)	Bi(2)–Br(5)	2.715(2)
Sb(2)–Br(3)	3.031(2)	Bi(2)–Br(3)	3.032(2)
Sb(1)–Sb(2)	3.933(2)	Bi(1)–Bi(2)	4.010(2)
P(1)–C(12)	1.757(19)	P(1)–C(12)	1.78(2)
P(1)–C(11)	1.89(3)	P(1)–C(11)	1.80(5)
P(2)–C(21)	1.63(4)	P(2)–C(21)	1.74(5)
P(2)–C(22)	1.760(18)	P(2)–C(22)	1.77(2)
P(3)–C(32)	1.746(5)	P(3)–C(32)	1.743(5)
P(3)–C(31)	1.909(19)	P(3)–C(31)	2.01(3)

the type of structure adopted by $[M_2X_9]^{3-}$ anions are following: the type of the halogen atoms, the size of the organic cations and the possibility of specific interactions with the anions. In the case of tetramethylammonium halogenoantimonates(III) and halogenobismuthates(III) discrete $[M_2X_9]^{3-}$ anions appears for bromine or mixed halogen analogs like: $[(CH_3)_4N]_3[Sb_2Br_9]$, $[(CH_3)_4N]_3[Sb_2Br_3Cl_6]$ [15]. Large organic cations and halogen atoms, and first of all, a lack of specific interactions of tetramethylammonium or tetramethylphosphonium cations with the anions may inhibit the formation of a polymeric anion.

The discrete dimeric structure for $[Sb_2Br_9]^{3-}$ or $[Bi_2Br_9]^{3-}$ in tetramethylphosphonium analogs is expected, since the phosphonium cations are distinctly larger than the corresponding alkylammonium ones. In general, the distortion of the anionic moieties of both bromine analogs is quite similar. Nevertheless, the subtle differences in the angle of the bioctahedral units of the PBA and PBB crystals are explained in terms of possible repulsion of the bromine atoms. The repulsion between the bridging atoms in the PBB compound diminishes and then the angle of Bi(2)–Br(3)–Bi(1), 82.67°, increases to a larger value than that of Sb(2)–Br(3)–Sb(1), 80.81°. A similar tendency is observed in some Br_t–M–Br_t (where Br_t are the terminal bromine atoms) angles. This phenomenon is also observed in closely related compounds, e.g. $[(CH_3)_4N]_3[Sb_2Br_9]$ [15] and $[(CH_3)_4N]_3[Bi_2Br_9]$ [18,19]. It means that the M–X_b–M angles (X_b—bridging halogen atoms) and M–M distance increase with increasing X–X repulsion (Sb–Sb 3.933 Å, Bi–Bi 4.010 Å). The remaining Br–Sb–Br and Br–Bi–Br angles change from 91.96(7) to 93.22(6) and from 91.74(7) to 93.34(7), respectively.

3.2. Thermal behavior of PBA and PBB

The DSC curves obtained for PBA and PBB crystals in the low- and high-temperature region during heating and cooling scans are presented in Fig. 3a and b, respectively. Hereafter, the following phase transition are denoted as phase (I), phase (II) and phase (III) from the high-temperature side. The calorimetric measurements revealed that both crystals undergo two reversible phase transitions, a high-temperature one, (I→II), continuous in nature, and a lower temperature one, (II→III), which is clearly of first-order type (discontinuous). The temperature of the phase transitions and the associated enthalpy and the entropy changes (ΔH and ΔS) are presented in Table 4.

According to Ptaszyński [20], the thermal decomposition of the antimony(III) complexes is, in general, a single-stage process resulting in the liberation of antimony tribromide and the appropriate amine or amine decomposition products. In our case the nature of the decomposition is complicated. Typical thermoanalytical curves, TGA and DTA, for one of the studied crystals (PBA) are reproduced in Fig. 4. The TGA curve of the PBA crystal indicates that it is thermally stable up to 620 K, when the continuous decomposition to the SbOBr begins. The DTA curve exhibits several events. The endothermic weak peak at 540 K corresponds to the reversible structural phase transition detected by the DSC measurements. The second endotherm with a peak at 700 K is accompanied by a loss in mass of about 30%. PBA decompose, probably, to SbOBr without an identifiable intermediate. The last exothermic peak at about 740 K is due to the decomposition of SbOBr.

Fig. 5 shows the results of the linear thermal expansion ($\Delta L/\Delta L_0$) measured along the main crystallographic axis of the trigonal system, *a* and *c*. It is seen that the sequence of the phase transition obtained by the dilatometric measurements is consistent with the calorimetric studies. It should be noted that the low-temperature anomalies in dilation for PBA and PBB along the *a* and *c* directions are positive. The step-wise changes in dimensions of crystal at the II→III phase transition temperature are comparable, being of the order of $0.5–1 \times 10^{-3}$ (the change in the *a*-direction for PBA is the most distinct). In the high-temperature region the anomalies in dilation at I→II phase transition of

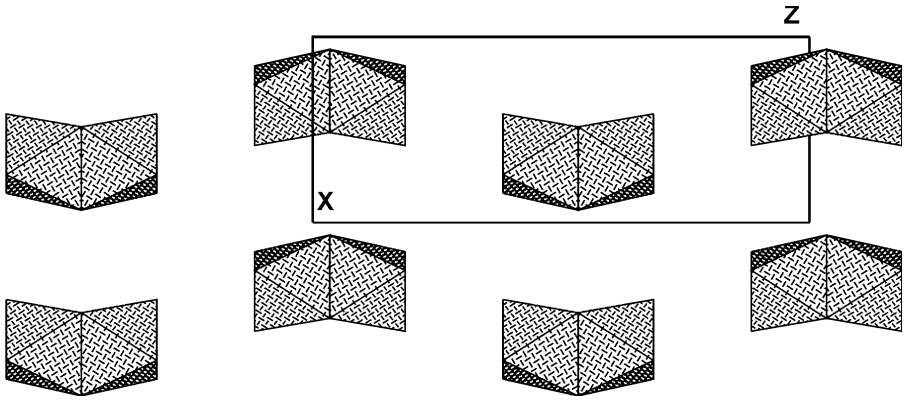

Fig. 2. Discrete $[Sb_2Br_9]^{3-}$ units in polyhedral representation along the *b*-axis.

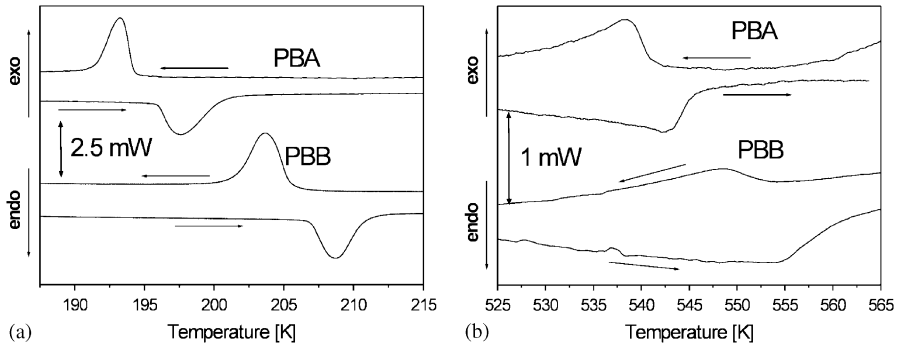

Fig. 3. DSC curves of the PBA and PBB crystals (a) for the low- and (b) high-temperature region for the cooling and heating runs (10 K min^{-1}).

Table 4
Structural phase transitions in $[(CH_3)_4P]_3[Sb_2Br_9]$ (PBA) and $[(CH_3)_4P]_3[Bi_2Br_9]$ (PBB) crystals detected by DSC and dilatometric measurements

Compound phase transition	PBA			PBB		
	T_c (K)	ΔT (K)	ΔS (J mol^{-1} K^{-1})	T_c (K)	ΔT (K)	ΔS (J mol^{-1} K^{-1})
I→II	540	—	—	550	—	—
II→III	193	2	8.5	205	2.5	10.6
	Dilatometry					
	Axis	$\frac{\Delta L}{L_0}$	$\frac{dT_c}{dp}$	Axis	$\frac{\Delta L}{L_0}$	$\frac{dT_c}{dp}$
II→III	*a*	4.7×10^{-3}	64×10^{-2}	*a*	2.8×10^{-3}	44.2×10^{-2}
	c	1.6×10^{-3}		*c*	2.6×10^{-3}	

T_c, ΔT and ΔS stand for the transition temperature (taken during cooling), temperature hysteresis and entropy of the phase transition, respectively. Lower part of the table—the changes of the linear thermal expansion along the *a* and *c* directions and the pressure coefficients dT_c/dp.

both crystals are quite similar and typical for the continuous transition. The pressure coefficient for this first-order phase transitions is estimated from the Clausius–Clapeyron relation:

$$\frac{dT_c}{dp} = \frac{\Delta V}{\Delta S}, \quad (1)$$

where ΔV denotes the change in the molar volume and ΔS is the value of the transition entropy. The magnitude of anomalies in dilation along the *a*- and *c*-axis and the pressure coefficients for PBA and PBB are listed in Table 4.

3.3. Dielectric and pyroelectric properties

To throw more light on the polar properties for PBA over the phases both above (phase II) and below 193 K (phase III) the pyroelectric measurements have been

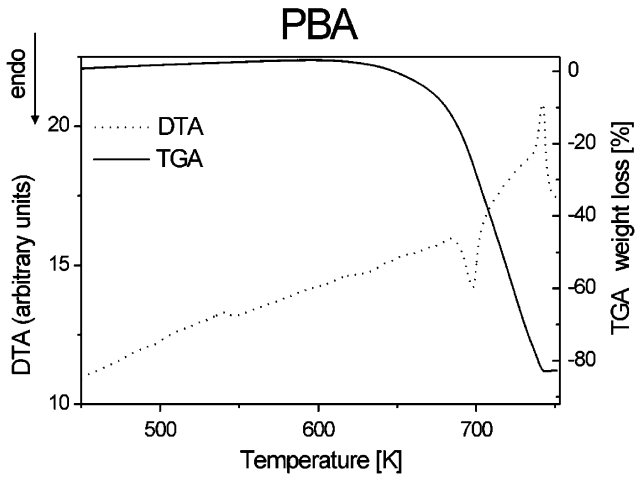

Fig. 4. Simultaneous thermogravimetric analysis and differential thermal analysis scan for PBA. The scan was performed in flowing nitrogen with a ramp rate of 2 K min^{-1} (selected single crystals, atmosphere: nitrogen, flow rate 1 dm^3 h^{-1}, weight 7.53 mg).

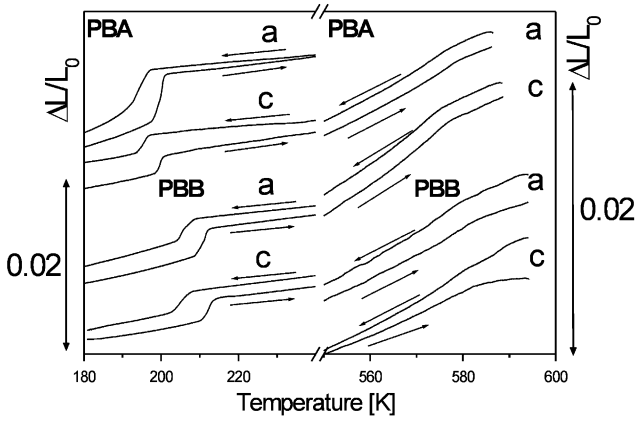

Fig. 5. Linear thermal expansion of the PBA and PBB crystals.

carried out. The pyroelectric current (I) and the spontaneous polarization change ($|\Delta P_s|$) as a function of temperature along the c- and a-axis (the notation of the axis is taken for the trigonal room temperature phase) is shown in Fig. 6. It is clearly seen that the spontaneous polarization change along the a-axis in the vicinity of 193 K is of the order of 2.5×10^{-5} C/m^2, which is several times larger than that observed along the c-axis. Unfortunately, it is not reversed under an external DC electric field. It should be emphasized that both phases are polar; nevertheless, there is no simple relationship between polar directions in each phase since the crystal undergoes a discontinuous phase transition. The measurements were also performed for the PBA along the c-direction. The $|\Delta P_s|$ in the vicinity of the transition at 205 K is comparable to that in PBB for the same direction.

It can be concluded that both PBA and PBB may be classified as a pyroelectric crystal both above and below 193 and 205 K, respectively, which supports the crystallographic results.

Fig. 7a and b shows the temperature dependence of the real and imaginary part of the complex electric permittivity, ε'_a, of the PBA crystal in the vicinity of the phase transition II→III at 193 K (on cooling) in the frequency region 75 kHz–10 MHz. This phase transition is accompanied by a relatively small step-wise dielectric anomaly. The upper part of Fig. 7a shows the electric permittivity ε' (at 25 MHz) along the c-axis of PBA in the close vicinity of 193 K. The transition along the c-direction is accompanied by a very weak dielectric anomaly seen as a step-wise increase in ε' without any visible dielectric losses in the vicinity of 193 K. On the other hand, over the intermediate phase (II) along the a-axis a characteristic shift of ε''_{max} with increasing frequency indicates a clear relaxation process. It has been found that the dielectric response in the PBA crystals is well described by the empirical Cole–Cole relation:

$$\varepsilon^* = \varepsilon_\infty + \frac{\varepsilon_0 - \varepsilon_\infty}{1 + (i\omega\tau)^{1-\alpha}}, \quad (2)$$

where ε_0 and ε_∞ are the low- and high-frequency limits of the electric permittivity, respectively, ω is the angular frequency, τ is the macroscopic relaxation time and α is a parameter of the distribution of relaxation times. An example of the Argand diagram at 240 K is presented in Fig. 7c. The macroscopic relaxation time reaches about 6×10^{-4} s at 240 K. Due to lack of experimental points on the low-frequency side of the diagram it is impossible to analyze the relaxation process in detail. The relaxation results indicate, however, a diffuse dielectric response with a possible distribution of relaxation times. The activation energy roughly estimated based on the Arrhenius relation is quite small, being of the order of 1 kJ/mol.

The real part of the complex electric permittivity, ε'_c, of the PBB crystal close to the phase transition temperature $T_{II\to III}$ (205 K) is shown in Fig. 7d. The phase transition is accompanied by a rapid decrease in the ε'_c approaching 205 K. This anomaly is visible only at frequencies below 10 kHz. A clear divergence in the electric permittivity of PBB observed over phase II may be connected to the conductivity phenomena associated with defects of the sample, which are characteristic of all samples of PBB. In our opinion this effect camouflages the expected relaxation process, which was observed in the PBA crystals.

3.4. Optical observations

Microscopic observations of the PBA and PBB crystals in the plane (001) (the directions correspond to those taken for the trigonal room temperature phase) showed an appearance of a phase front at 193 or 205 K

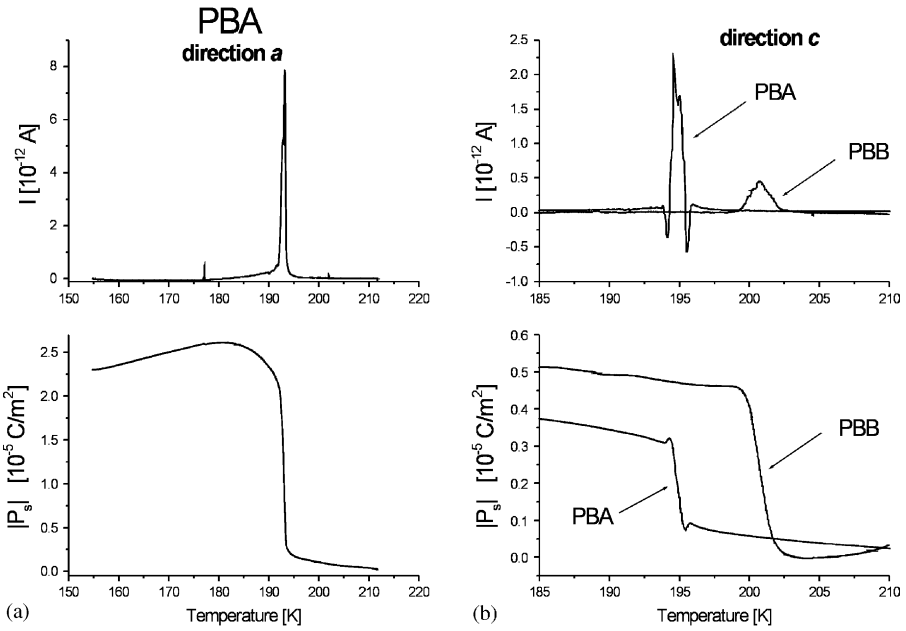

Fig. 6. The temperature dependence of the spontaneous polarization change, $|\Delta P_s|$, and pyroelectric current, I_{pyro}, for (a) the PBA crystal along the a-axis and (b) for the PBA and PBB crystals along the c-axis.

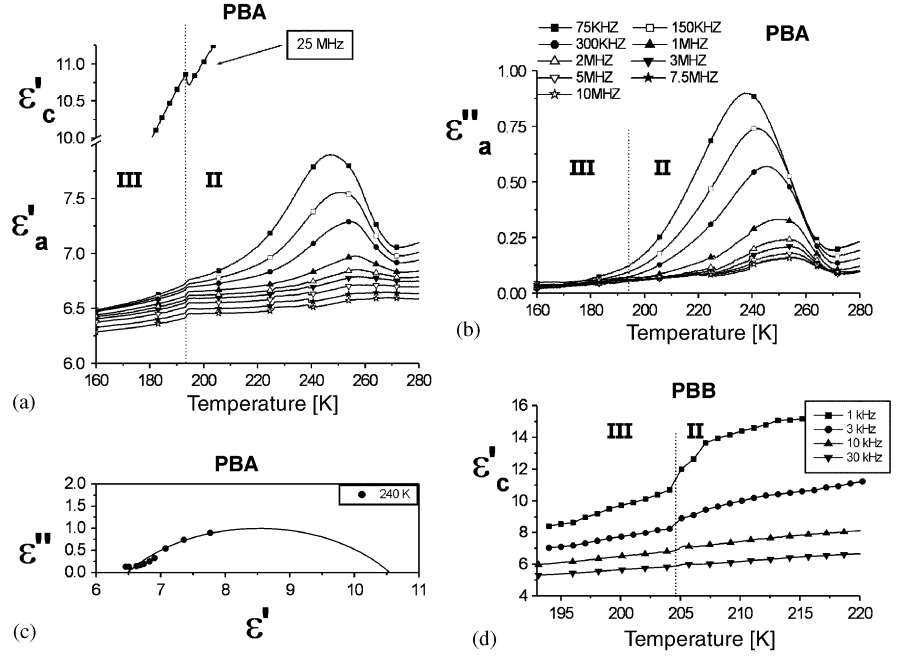

Fig. 7. (a), (b) Temperature dependence of the real (ε'_a) and imaginary (ε''_a) part of the complex electric permittivity (ε^*), of PBA in the vicinity of the II→III phase transition between 75 kHz and 10 MHz. The upper part of Fig. 7a shows the temperature dependence of ε'_c at 25 MHz. (c) Cole–Cole diagram for the PBA crystal at 240 K. (d) Temperature dependence of ε'_c for PBB close to the T_c (II→III) transition temperature between 1 kHz and 30 kHz.

corroborating the discontinuous character of the II→III phase transition for PBA and PBB, respectively. Below this temperature a fine domain structure developed. This process is perfectly reversible. It clearly confirms that these transitions may be classified as a ferroelastic one. In phase (III) of both crystals (see Fig. 8a and c) domain boundaries being crossed with the angle of 60° and 120° are seen. The observed domain walls of type W are oriented along the [100] direction (see Fig. 8b and d). The domain walls of type W' run nearly perpendicular to the [100] direction. This observation indicates that this phase transition is accompanied by a change in the crystal symmetry. No change in the domain pattern is observed over the phase (III) down to 77 K.

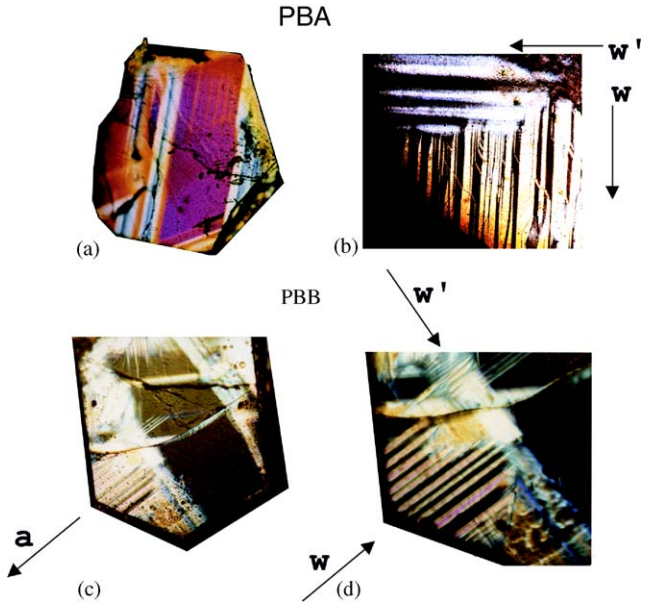

Fig. 8. A micrograph of ferroelastic domains of PBA (at 180 K) and PBB (at 190 K) between crossed polarizers taken in the (001) plane.

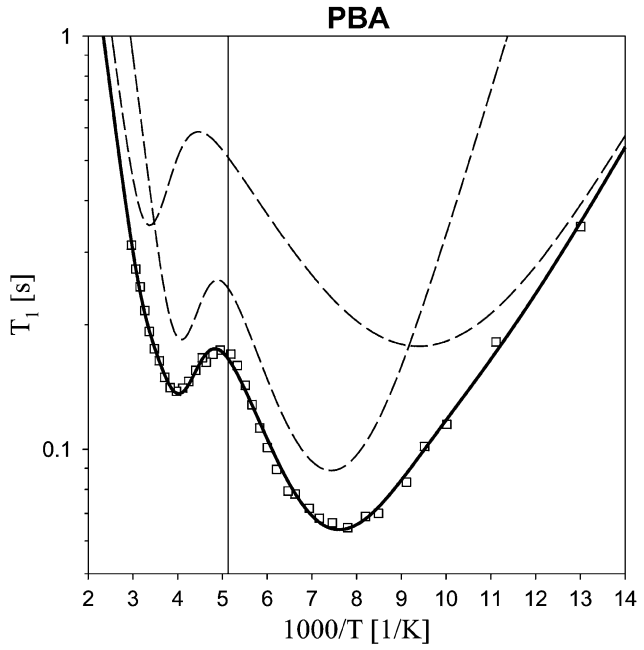

Fig. 9. A semilog plot of the temperature dependence of the proton spin–lattice relaxation time (T_1) of the PBA crystal at 90 MHz over phases (II) and (III). The solid line is a result of the fit of Eqs. (3) and (4), and broken lines correspond to both components of Eq. (3).

Based on the optical observations and Sapriel's approach [21] one can state that the PBA and PBB crystals belong to the ferroelastic species with $3mFm$ or $3mF1$ domain pattern.

3.5. ^{1}H *NMR measurements*

The proton magnetic resonance technique has been used to study the cationic dynamic in the PBA crystal in temperatures 77–400 K. The proton spin lattice relaxation times (T_1) obtained over the ferroelastic phase (III) and paraelastic phase (II) are shown in Fig. 9 as semilog plots versus inverse temperature. Upon heating, two well-defined but asymmetrical T_1 minima (64 ms at ca. 128 K and 138 ms at ca. 251 K) are disclosed. It should be noted that these two minima are separated by the phase transition point at 193 K. It is clear that no discontinuous anomaly in the vicinity of the phase transition in PBA at 195 K is visible in the T_1 measurements. It means that the dynamical state of the tetramethylphosphonium cations is practically unchanged when the II→III phase transition takes place. The asymmetrical shape of the observed minima led us to the conclusion that in the studied compound the inequivalence of the cations occurs. In such a case it was assumed that the total relaxation rate is approximated by the equation [22]:

$$\frac{1}{T_1} = \frac{N_A}{N}\frac{1}{T_{1A}} + \frac{N_B}{N}\frac{1}{T_{1B}}, \tag{3}$$

where T_{1A} and T_{1B} denote the relaxation times of the protons of A and B type cations; N_A and N_B with $N = N_A + N_B$ denote the numbers of the protons of the tetramethylphosphonium cations of type A and B, respectively. In the studied case $N_A = 1$ and $N_A = 2$. The T_{1A} versus temperature dependence was analyzed with the BPP theory, where it was assumed that two kinds of motions of the cation appear: the CH_3 reorientation about its C_3-axis and the overall reorientation of the cation. These two motions could be regarded as separable from each other. If the correlation times of the proposed motions are expressed as τ_1 and τ_2, respectively, the cation relaxation time is given by [23]:

$$\frac{1}{T_1} = \frac{9}{20}\frac{\gamma^4\hbar^2}{r_{CH_3}^6}\left(\frac{\tau_3}{1+\omega_0^2\tau_3^2} + \frac{4\tau_3}{1+4\omega_0^2\tau_3^2}\right) + \gamma^4\hbar^2\left(\frac{3}{20}\frac{1}{r^6} + \frac{27}{10}\frac{1}{R^6}\right)\left(\frac{\tau_2}{1+\omega_0^2\tau_2^2} + \frac{4\tau_2}{1+4\omega_0^2\tau_2^2}\right), \tag{4}$$

where $\tau_3^{-1} = \tau_1^{-1} + \tau_2^{-1}$. In this equation ω_0 and γ represent the resonance angular frequency and the magnetogyric ratio of a proton, respectively, and r and R denote the interproton distance in the methyl CH_3 group and the distance between the centers of each regular triangle formed by three protons of each four CH_3 groups in the cation, respectively. The temperature dependence of the correlation times in the temperature range of the fit is described by the Arrhenius law:

$$\tau = \tau_0 \exp(E_a/RT), \tag{5}$$

where τ_0 is the correlation time at the limit of infinite temperature. The values of the E_a and τ_0 obtained by

Table 5
Activation parameters for the cation motions in the PBA crystal

$[(CH_3)P]^+$ cation	Motion	E_a (kcal mol^{-1})	τ_0 (s)
A	The C_3 rotation of the CH_3 group	0.8	2.0×10^{-11}
	overall reorientation	5.1	2.0×10^{-13}
B	The C_3 rotation of the CH_3 group	1.6	2.4×10^{-12}
	overall reorientation	5.1	3.9×10^{-14}

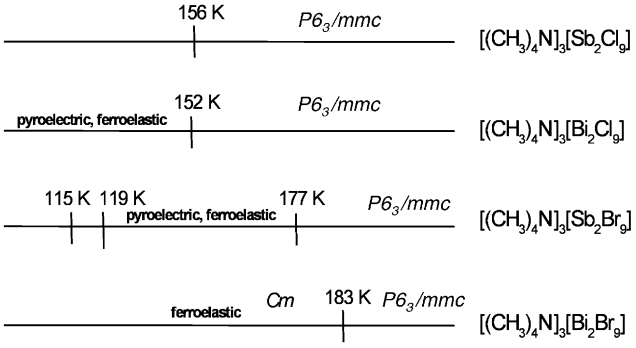

Fig. 10. Phase situation in tetramethylammonium crystals.

use of the measured T_1 data and Eqs. (3)–(5) are shown in Table 5 for the assigned motions of both inequivalent cations. In summary, the T_1 measurements on the PBA have shown that phase (II) and phase (III) are characterized by various motional states of the two inequivalent $[(CH_3)_4P]^+$ cations. Over the lowest temperature phase (III) only the C_3-type of motion of the methyl group is suggested, whereas over the intermediate phase (II) the overall reorientation of these cations takes place.

4. Discussion

The closely related tetramethylammonium analog, $[(CH_3)_4N]_3[M_2X_9]$ ($M = Sb$, Bi and $X = Cl$, Br), crystallize in the hexagonal space group, $P6_3/mmc$. Refinement for the bromine compound, $[(CH_3)_4N]_3[Sb_2Br_9]$ ($R = 0.14$), was very poor, probably as a consequence of disorder of tetramethylammonium cations. In spite of this, a clearly confacial bioctahedral structure of the anionic moieties was found in the bromine compounds. Comparison of the phase situation found in the tetramethylammonium analogs with that discovered by present measurements seems to be instructive. The phase transition sequence that appears in the $[(CH_3)_4N]_3[M_2X_9]$ [24,25] subgroup is illustrated in Fig. 10. The altering of the quaternary organic cation in the system $[(CH_3)_4Z]_3[M_2X_9]$ ($Z = N$, P, As, Sb), where the central nitrogen atom of the cation is replaced by higher members of the pnicogen group e.g. the P atom, does not lead to any significant differences in the structure of the anionic sublattice. Both subgroups, $[(CH_3)_4N]_3[M_2X_9]$ and $[(CH_3)_4P]_3[M_2X_9]$, are characterized by discrete bioctahedral anionic units. The title phosphonium compounds, PBA and PBB, show phases similar in several respects to their tetramethylammonium analogs. The common feature is the disorder forced on the cations by the space group symmetry ($P31c$ or $P6_3/mmc$) in the room temperature phases. The freezing of motion of the cations leads to low-temperature ordered phases. The low-temperature phase transitions are usually accompanied by a distinct distortion of the anionic sublattice that is probably the reason for the appearance of ferroelastic properties. It should be emphasized that the most attractive feature of the tetramethylammonium or tetramethylphosphonium halogenoantimonates(III) and halogenobismuthates(III) is the appearance of polar (pyroelectric) properties.

On the basis of X-ray, calorimetric, ^{1}H NMR and dielectric responses the following change in the dynamics of molecules with temperature in the tetramethylphosphonium compounds may be proposed. The NMR studies showed that in the lowest temperature phase (III) the organic cations are "frozen" as a whole having only the C_3-type motion of the methyl groups. Approaching the III→II phase transition temperature from below the onset of the isotropic reorientation of the cations is the most probable. This model seems to be partially confirmed by the present dielectric studies on PBA. The crystal lattice consists of $[(CH_3)_4P]^+$ cations and $[Sb_2Br_9]^{3-}$ anions.

Taking into account the values of the isotropic displacement coefficients (U_{eq}) of the carbon atoms of the cations, it is not surprising that the low-temperature phase transition in both analogs involves reorientation of the $[P(CH_3)_4]^+$ cation. However, the situation for the three types of cations seems to be different. The U_{eq} parameters of the carbon atoms of the cations type (1) and type (2), being of the order of 0.10–0.14 Å^2 suggest only the libration of these cations in the room temperature phase (II). In turn, for cations type (3) these parameters are nearly twice as large as for type (1) and type (2). This clearly shows that the methyl groups (C31 and C32 for both PBA and PBB) are disordered over several sites. Such a model of disorder of the cations seems to be consistent with the calorimetric data, showing a significant entropy transition value for the low-temperature transition ($\Delta S = 8.5$ (PBA) and 10.6 J mol^{-1} K^{-1} (PBB)). Assuming that only one (type (3)) of the three nonequivalent cations contributes to the

mechanism of the low-temperature phase transition the entropy transition indicates the isotropic reorientation of this cation over phase II and a drastic diminishing of this motion below the transition point. It should be added that the distribution of the macroscopic relaxation times observed over the intermediate phase (II) may be explained in terms of the dynamical nonequivalence of the $[(CH_3)_4P]^+$ cations shown by X-ray studies. The observed dielectric relaxation mode in the $[(CH_3)_4P]_3[Sb_2Br_9]$ and $[(CH_3)_4N]_3[Bi_2Cl_9]$ [24] and assigned to the ordered $[(CH_3)_4Z]^+$ cations is also confirmed by our spin–lattice relaxation measurements (^{1}H NMR).

Comparing dielectric properties of tetramethylammonium and tetramethylphosphonium compounds belonging to the family $[(CH_3)_4Z]_3[M_2X_9]$ ($Z = N, P$, M = Sb, Bi), one should observe that all first-order phase transitions taking place in the low-temperature region are usually accompanied by a relatively small change in the electric permittivity. The electric dipole–dipole interactions between organic cations that bestowed quite small permanent dipole moment is rather weak. Thus, one could conclude that its contribution to the electric increment ($\Delta\varepsilon$) in the vicinity of T_c is negligible. These small changes in the $\Delta\varepsilon$ at the critical point are mainly due to the alterations of density of crystals.

Concluding the dielectric and pyroelectric studies on the $[(CH_3)_4Z]_3[M_2X_9]$ ($Z = N, P, As, Sb$) family of crystals one can state that the analogous character of the dielectric response and pyroelectric characteristics of all compared crystals indicates a similar mechanism of the phase transitions.

It might be interesting to compare the entropy changes accompanying the phase transitions in the title crystals with those observed in the $[(CH_3)_4N]_3[M_2X_9]$ salts. PBA and PBB revealed the entropy changes $\Delta S \approx 8$–$10\ J\ mol^{-1}\ K^{-1}$ per three cations, whereas the corresponding (ferroelastic) phase transitions in tetramethylammonium salts exhibited [25–27]: $[(CH_3)_4N]_3[Sb_2Cl_9]$—10.5, $[(CH_3)_4N]_3[Sb_2Br_9]$—11.0, $[(CH_3)_4N]_3[Bi_2Cl_9]$—8.9, $[(CH_3)_4N]_3[Bi_2Br_9]$—14. Assuming a two-site model with the corresponding entropy effect of the order of $R\ln 2 = 5.76\ J\ mol^{-1}K^{-1}$ one can suggest that at least one or two cations, for all crystals, are involved in the phase transition mechanism of an order–disorder type.

In summary one can state that the mechanism of the paraelastic–ferroelastic (II→III) phase transition is complex. Dynamics of the organic cations is connected with the order–disorder contribution. The appearance of ferroelasticity may be explained in terms of the shift of the anionic sublattice with respect to the cationic one. This mechanism may be treated as a "displacive" contribution.

References

[1] R. Jakubas, L. Sobczyk, Phase Transitions 20 (1990) 163.
[2] L. Sobczyk, R. Jakubas, J. Zaleski, Pol. J. Chem. 71 (1997) 265.
[3] B. Mróz, J.A. Tuszyński, H. Kiefte, M.J. Clouter, R. Jakubas, D. Sept, Phys. Rev. B 58 (1998) 14261.
[4] T. Kawai, E. Takao, S. Shimanuki, M. Iwata, A. Miyashita, Y. Ishibashi, J. Phys. Soc. Jpn. 68 (1999) 2848.
[5] M. Hashimoto, S. Hashimoto, H. Terao, M. Kuma, H. Niki, H. Ino, Z. Naturforsch. 55a (2002) 167.
[6] M. Wojtaś, G. Bator, R. Jakubas, J. Zaleski, B. Kosturek, J. Baran, J. Solid State Chem. 173 (2003) 425.
[7] R. Jakubas, Z. Czapla, Z. Galewski, L. Sobczyk, O.J. Żogal, T. Lis, Phys. Stat. Sol. A 93 (1986) 449.
[8] A. Kallel, J.W. Bats, Acta Crystallogr. C 51 (1985) 1022.
[9] F. Lazarini, Acta Crystallogr. B 33 (1977) 2686.
[10] J. Jóźków, R. Jakubas, G. Bator, A. Pietraszko, J. Chem. Phys. 114 (2001) 7239.
[11] R. Jakubas, G. Bator, Z. Ciunik, Phys. Rev. B 64 (2003) 024103.
[12] A. Pietraszko, R. Czopnik, R. Jakubas, Phys. Rev. B, submitted.
[13] G.M. Sheldrick, SHELXS-97, Program for the solution of crystal structure, University of Göttingen, Germany, 1997.
[14] G.M. Sheldrick, SHELXL-97, Program for the Refinement of Crystal Structure, University of Göttingen, Germany 1997.
[15] M. Hall, M. Nunn, M.J. Begley, D.B. Sowerby, J. Chem. Soc. Dalton Trans. (1986) 1231.
[16] C.H. Hubbard, R.A. Jacobson, Inorg. Chem. 11 (1972) 2247.
[17] F. Lazarini, Acta Crystallogr. B 33 (1977) 2686.
[18] H. Ishihara, K. Watanabe, A. Iwata, K. Yamada, Y. Kinoshita, T. Okuda, V.G. Krishnan, S. Dou, A. Weiss, Z. Naturforsch. 47a (1992) 65.
[19] H. Ishihara, K. Yamada, T. Okuda, A. Weiss, Bull. Chem. Soc. Jpn. 66 (1993) 380.
[20] B. Ptaszyński, Thermochim. Acta 197 (1992) 335.
[21] J. Sapriel, Phys. Rev. B 12 (1975) 5128.
[22] D.E. Woessner, J. Chem. Phys. 36 (1962) 1.
[23] S. Albert, H.S. Gutowsky, J.A. Ripmeester, J. Chem. Phys. 56 (1972) 3672.
[24] R. Jakubas, G. Bator, J. Mróz, Acta Phys. Pol. 87 (1995) 663.
[25] R. Jakubas, Z. Galewski, L. Sobczyk, J. Matuszewski, Ferroelectrics 88 (1988) 83.
[26] W. Medycki, R. Jakubas, N. Piálewski, J. Lefebvre, Z. Naturforsch. 48a (1993) 748.
[27] R. Jakubas, Z. Galewski, J. Matuszewski, J. Lefebvre, Phys. Stat. Sol. A K19 (1993) 136.